Short Communication

Effect of double-hit deformation on the onset of critical stress for the initiation of dynamic transformation

K. Chadha[1*], C. Jr. Aranas[2], M. Zaid Ahmed[3], M. Jahazi[4], J.G. Spray[1]

[1]Planetary and Space Science Centre, University of New Brunswick
Fredericton, New Brunswick E3B 5A3, Canada
[2]Department of Mechanical Engineering, University of New Brunswick
Fredericton, New Brunswick E3B 5A3, Canada
[3]Regional Technological Institute University of West Bohemia, Plzeň, 30100, Czech Republic
[4]Department of Mechanical Engineering, École de technologie supérieure (ÉTS),
1100 Notre Dame Street West, Montréal, Québec H3C 1K3, Canada
*Corresponding author: Kchadha@unb.ca

Abstract

Double-hit hot compression tests were carried on medium-carbon low-alloy steels using Gleeble 3800® thermomechanical simulator. The tests were performed at strain rates of 0.25 and 0.5 s^{-1} and temperatures of 1150 and 1200 °C with an interpass time of 5s. The onset of critical stress for dynamic transformation (DT) were detected using the double-differentiation method. This metallurgical phenomenon was initiated under all testing conditions. The results show that the critical stress for DT increases with decrease in temperature and increase in strain rate.

Keywords: Dynamic Transformation; Thermomechanical Processing; Double-hit deformation.

Introduction

The final property of the forged ingot is dependent on the chronicle of the deformation process. The forging process begins with an as-cast ingot which has microstructural and chemical inhomogeneities. Understanding the evolution of the phases during the high-temperature deformation process is very essential. In the manufacturing industry, more than one hit is applied

to give the as-cast ingot a final shape. During this deformation process, various dynamic softening processes occur, amongst which are dynamic transformation (DT) and dynamic recrystallization (DRX)[1]. The occurrence of DT was first reported by Yada et al.[2, 3] in the 1980s. They investigated the progress of DT under both laboratory testing conditions and pilot rolling mill trials. Later, they were able to follow the phenomenon in real-time when they deformed steel samples via torsion testing in an X-ray diffraction apparatus. Since then, several researchers have since studied both the forward and reverse transformations till date [4-8].

The initiation of DT and DRX usually occur at a particular strain known as the critical stress (σ_c) and their related strains are known as critical strain (ε_c) [9]. As DT and DRX are flow softening mechanisms, they usually lead to a reduction in the net work-hardening rate as related to the values anticipated when only dynamic recovery is taking place. However, the flow softening is relatively insignificant at the critical strains since very minute volume fraction of ferrite and recrystallized austenite form during this stage. Therefore, the flow stress further increases beyond these critical strains until the softening due to the effect of DT and DRX is balanced by the strain hardening taking place simultaneously in the undeformed material. After this, steady state stress is achieved, which is the final balance between the rates of hardening and softening [10].

The peak in the flow curve is usually a good indication that a softening process occurred. However, it does not provide any evidence about the exact initiations of DT or DRX. Such critical stress can be successfully determined using the double differential technique developed by Poliak and Jonas [11, 12]. The method involves the determination of the critical stress (and its corresponding strain) from the point of inflection in a plot of the strain hardening rate as a function of the stress. Since most of the extensive analysis of critical strains in the literature involves single hit experiments, in the current work, the double differentiation technique is applied to the flow stress data of double hit deformed medium carbon low alloy steel, processed at two temperatures, two strain rates and one interpass time. The dependence of critical stresses and strains on temperature and strain rate to initiate DT and DRX (complemented with microstructural analysis) are presented.

Experimental

The composition of the steel used for the experiments is shown in Table 1, along with its ortho-equilibrium and para-equilibrium Ae_3 temperatures. These values were calculated using the FactSage thermodynamic software, employing the FSStel Database® [13]. Materials were provided by Finkl Steel-Sorel, Canada. Cylindrical specimens were machined from the central region of the as-cast ingot with diameters and heights of 10 mm and 15 mm, respectively. Hot compression tests were performed using a Gleeble 3800® thermomechanical simulator following the procedures described in ASTM E209. The schematic diagram for double-hit compression tests is shown in Fig. 1. Two temperatures (1200 °C and 1150 °C), two strain rates (0.25 s^{-1} and 0.5 s^{-1}), and one interpass time (5 s) were employed in the experiments.

Table 1: Composition of medium-carbon low-alloy steel.

C	Mn	Si	Mo	Cr	Other	Ae_3 Temperature
0.35	0.84	0.41	0.44	1.90	Microalloying	756 °C

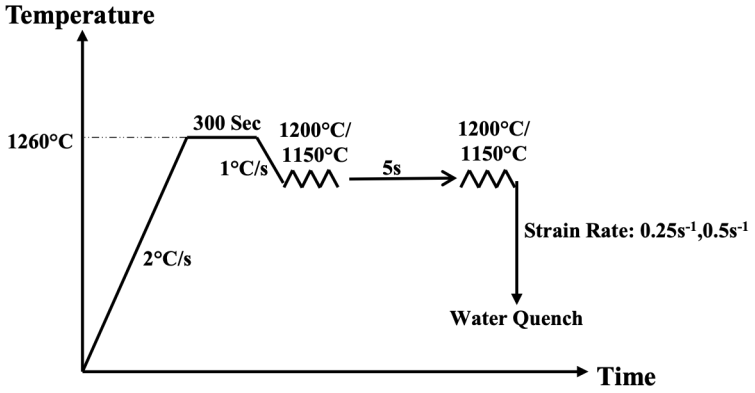

Figure 1: Schematic diagram of thermomechanical schedule for double hit hot compression tests of medium-carbon low-alloy steel

The thermomechanical procedure consisted of heating the sample to 1260 °C at a heating rate of 2 °C/s and soaking for 5 minutes (300 s) to homogenize the temperature and the microstructure. The samples were then cooled to the deformation temperature at a rate of 1 °C/s before being compressed to a total true strain of 0.8. The first deformation (first hit) was applied till a true strain of 0.5 followed by 5 s interpass time. The second pass (second hit) was then applied till a true strain of 0.3 followed by water quenching. The samples were mechanically polished using conventional metallographic preparation techniques and final polished using a Vibromet® polisher. Each sample was then placed in the SEM chamber with its compression axis parallel to the incident electron beam. The EBSD analysis was performed using a Hitachi SU-70 field emission gun scanning electron microscope equipped with Schottky emitter. Post-processing was done using Channel 5 HKL^{TM} software. Low-angle grain boundaries (LAGBs, $\theta < 2°$) are marked red, while high-angle grain boundaries (HAGBs, $\theta > 15°$) are labeled black.

Results

The flow curves obtained from the double-hit deformation at 1200 °C and 1150 °C and strain rates of 0.25 s^{-1} and 0.5 s^{-1} and the interpass time of 5s are displayed in Fig. 2. Note that this temperature is approximately 450 °C and 400 °C above the para-equilibrium Ae_3 temperature of the alloy. As expected, the results show that the stress levels increase with strain rate and temperature. After the first deformation, both flow curves show a steady increase in stress and then gradually decrease after a peak stress of 58.2 MPa and 63.8 MPa for strain rates of 0.25 and 0.50 s^{-1} (at 1200 °C), respectively. Similarly, at 1150 °C, peak stresses of 74.1 MPa and 81.2 MPa were recorded followed by gradual decrease in stress for strain rates of 0.25 and 0.50 s^{-1}, respectively. During the second deformation, a peak stress drop of about 15% (compared to the first deformation) can be seen for both testing temperatures. These results reveal that dynamic softening has taken place during the 5 s time interval

It is well recognized that during hot deformation of medium-carbon low-alloy steels, in addition to DRX, the DT of austenite to ferrite also occur. The kinetics of DT is much faster than DRX [14]. The double differentiation technique, proposed by Poliak and Jonas [12, 15], was used to evaluate the critical strains and stresses for the initiation of both DT and DRX. A dedicated script was developed in MATLAB® for analyzing the flow curves using this method.

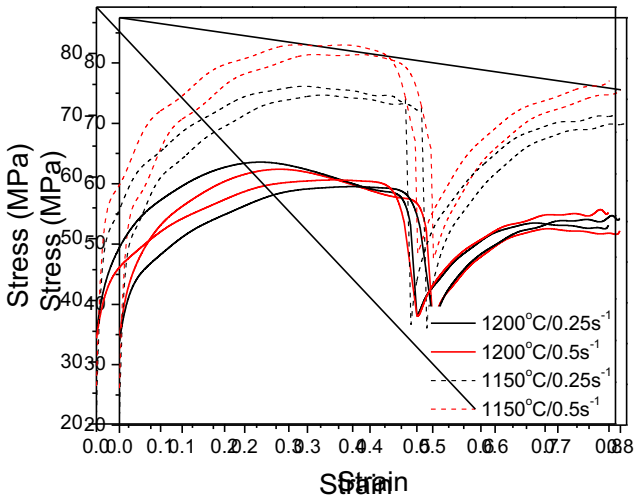

Figure 2: Stress strain curve of medium-carbon low-alloy steel deformed at 1200 °C and 1150 °C and strain rate of 0.25 s^{-1} and 0.5 s^{-1} with an interpass time of 5s.

In every instance, a "yield stress" was first found as a 2% offset in the total strain. This was considered to represent the commencement of macroscopic work hardening in compression. After the removal of this "microplastic" part, each curve was fitted and smoothed with a 10^{th}-order polynomial using the MATLAB™ software. In some challenging cases, a higher-order polynomial (14^{th}) was employed. The smoothing eliminated the fluctuations present in the experimental flow curves and in this way, allowed the differentiation operations.

In order to determine the critical stresses for the initiation of DT and DRX, the strain hardening rate, θ, was calculated by the following expression:

$$\theta = \left(\frac{\delta\sigma}{\delta\varepsilon}\right)_{\dot{\varepsilon}} \quad (1)$$

The minima were then calculated by taking the derivative of θ, [9, 10], as described by the equation below:

$$\left(\frac{\delta}{\delta\sigma}\right)\left(\frac{\delta\theta}{\delta\sigma}\right)=0 \quad (2)$$

Therefore, according to Equation 2, the onsets of DT and DRX are associated with inflection points in a $\theta - \sigma$ plot and with minima in a $-(\partial\theta/\partial\sigma)$ versus σ curve. In most cases, there are two inflection points, the first of which indicates the onset of DT and the second is the initiation of DRX.

The $-(\partial\theta/\partial\sigma)$ versus σ curves for the first hit and second hit for medium-carbon low-alloy steel at various experimental temperatures and strain rates are shown in Figs. 3 a and 3 b, respectively. The two minima displayed in Figs. 3 represent the critical stresses at which DT were initiated during deformation. The graph in Fig. 4 show the dependence of DT critical stress versus temperature and strain rate. It can be seen that with the increase in temperature the critical stresses for DT decreases in both first and second hit deformation, whereas, the critical stress for DT increases with strain rate for both first and second hit deformation.

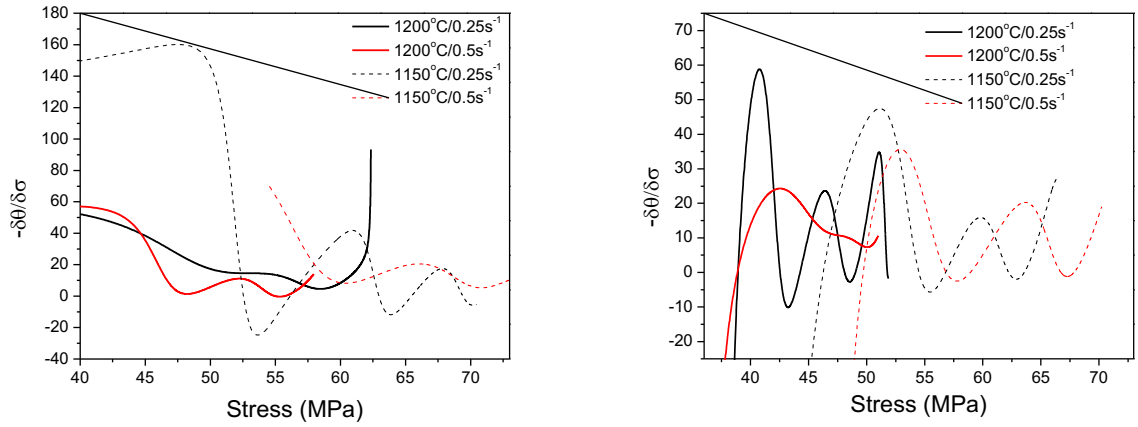

Figure 3: Double differential minima curves at deformation temperature of 1200 °C and 1150 °C and strain rates of 0.25 s^{-1} and 0.5 s^{-1} for (a) first hit and (b) second hit deformation.

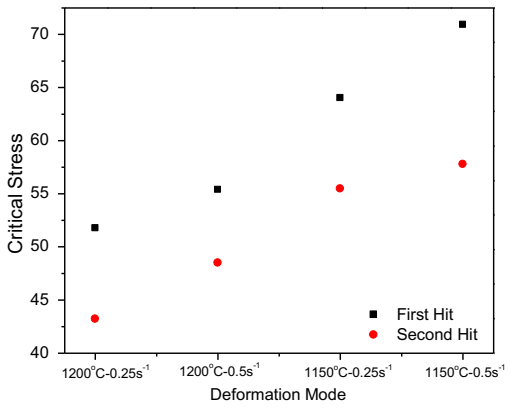

Figure 4: Variation of critical stress for the initiation of DT with respect to the deformation mode.

Considering that the double differentiation technique involves purely mathematical findings, microstructural analysis is needed to validate the presence of dynamically transformed ferrite, as presented below.

Fig. 5 a show the grain boundary map of the specimen after double hit deformation at 1150 °C and a strain rate of 0.25 s^{-1}. A detailed observation of the microstructures shows a morphology composed of laths and few quasi-polygonal grains (indicated with red arrows). The plates observed in the microstructure appear to have Widmanstätten type morphology, which originates from the interior of the prior austenite grains. This observation is consistent with the results of numerous researchers [1, 16, 17] who linked their formation to the applied stress, which stimulates the displacive transformation of austenite to Widmanstätten ferrite.

EBSD grain boundary maps, reported in Fig. 5 (a) shows that a significant amount of low-angle grain boundaries is present in the microstructure. This indicates that the microstructure is not fully recovered after the second hit. However, the presence of any LAGBS was not found in the laths and plates, which suggests that these grains underwent recrystallization and phase transformation.

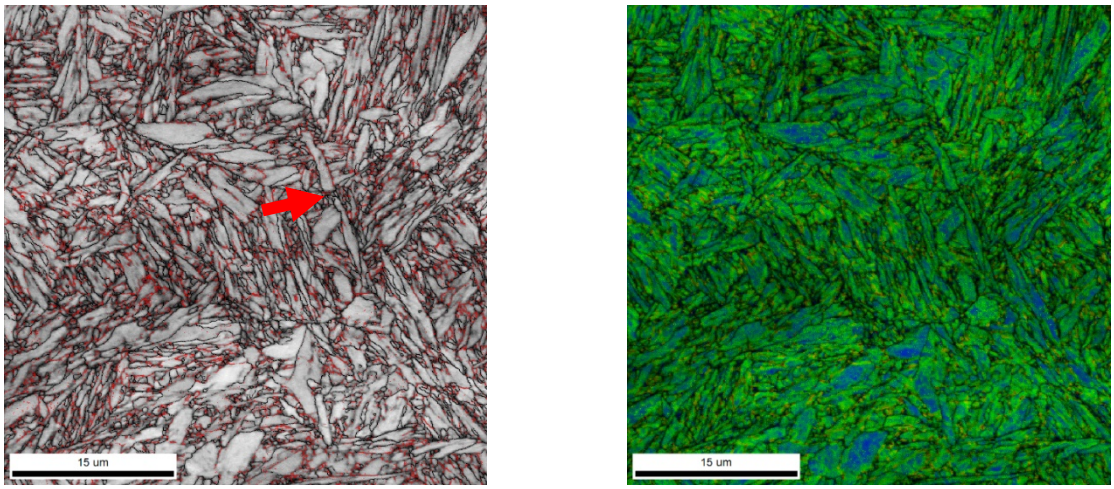

(a) (b)

Figure 5: (a) EBSD grain boundary map of medium-carbon low-alloy steel deformed at deformation temperature of 1150 °C and strain rate of 0.25 s^{-1}. Black lines denote HAGB and red lines denote LAGB. (b) EBSD Kernal Average Map (KAM) of medium-carbon low-alloy steel deformed at deformation temperature of 1150 °C at strain rate of 0.25 s^{-1}. Black lines denote HAGB.

Since, it is challenging to differentiate between martensite and DT ferrite using XRD, optical microscopy, or secondary electron imaging, the present study employed the Kernal Average Misorientation (KAM) method [7]. In this method, internal misorientation between grains is used to differentiate the martensite (body-centered tetragonal) from the ferrite (body-centered cubic) by the method of EBSD images. Up to the third nearest neighbor was considered for calculating KAM values, and a threshold angle of 5° was used. To study the recovery behavior, only the area fractions with less than 2° misorientation (i.e., KAM ≤ 2°; green and blue regions) were considered. Using the above criteria, the dynamic recovery process of the two phases was studied, and a distinction was successfully made between ferrite and martensite. It is known that ferrite has a higher stacking fault energy (SFE) [18] than austenite, which would make dynamic recovery simpler when it is further deformed to a higher strain (ε=0.8). Conversely, martensite laths (from prior austenite), which are formed due to shape deformation (displacive transformation), generate a higher amount of LAGBs, resulting in higher misorientations within the laths.

Fig. 5 b shows the KAM map for the specimen deformed at 1150 °C and at a strain rate of 0.25 s^{-1}. Widmanstatten ferrite plates, as seen on the Grain Boundary map of Fig. 5 a, have <2° misorientation (see Fig. 5 a), thus proving that they are recovered ferrite grains. Conversely, grains

with KAM values between 3°-5° indicate the presence of martensite. The volume fraction of dynamically transformed ferrite is 72% for 1150 °C and 0.25 s^{-1}.

Fig. 6, shows the phase map of specimen deformed at 1200 °C and a strain rate of 0.25 s^{-1}. This sample was strained till 0.5 strain and then held for 5 s interpass time at temperature of 1200 °C and water quenched to preserve the microstructure. The yellow color represents ferrite (BCC phase) and red color represents austenite (FCC phase). It can be seen that the austenite is present in trace amounts in the ferrite phase. The phase fraction of austenite is 4.2 % and that of ferrite is 95.8%. The austenite present in this specimen is due to re-transformation from ferrite to austenite during interpass time [1].This re-transformation happens by a diffusional transformation.

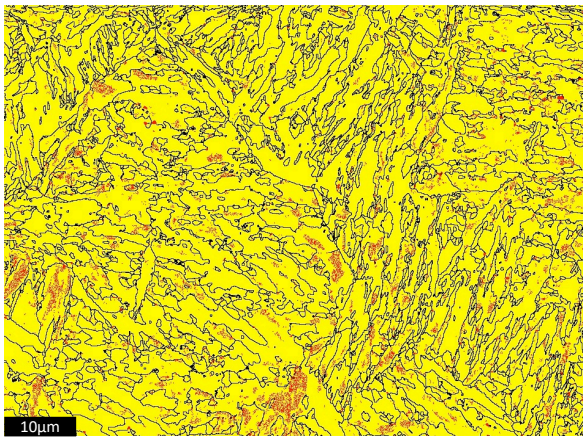

Figure 6: Phase map of a sample deformed at 1200 °C and strain rate of 0.25 s^{-1} deformed till a strain of 0.5 and then held for 5s at 1200 °C. Yellow color denotes ferrite phase and red denotes austenite phase.

To understand the mechanism behind the transformation during double-hit scenario, a schematic diagram is proposed as shown in Fig. 7. It is known that the austenite to ferrite transformation occurs due to energy supplied by the applied stress as reported in Ref [19]. Once the energy is above the total energy obstacles, which consist of the free energy difference between the phases, and the works of shear accommodation and lattice dilatation, transformation can take place. However, upon isothermal holding, re-transformation process can take place. This reverse transformation normally requires more than 60s of holding time to fully transform the DT ferrite back into austenite by diffusional mechanism. However, when the holding time to allow for re-transformation is short, e.g., 5 s in the present case, a partial re-transformation occurs that leads to trace amounts of re-transformed austenite to be formed along with DT ferrite. Therefore, during

the second hit deformation, the austenite transforms into ferrite in a similar manner with the first deformation, which involves a driving force supplied by the applied stress. During this process, the dynamic recrystallization of ferrite which was formed during the previous deformation hit can also occur. Thus, the overall effect leads to lower critical stress for the onset of DT during the second hit deformation.

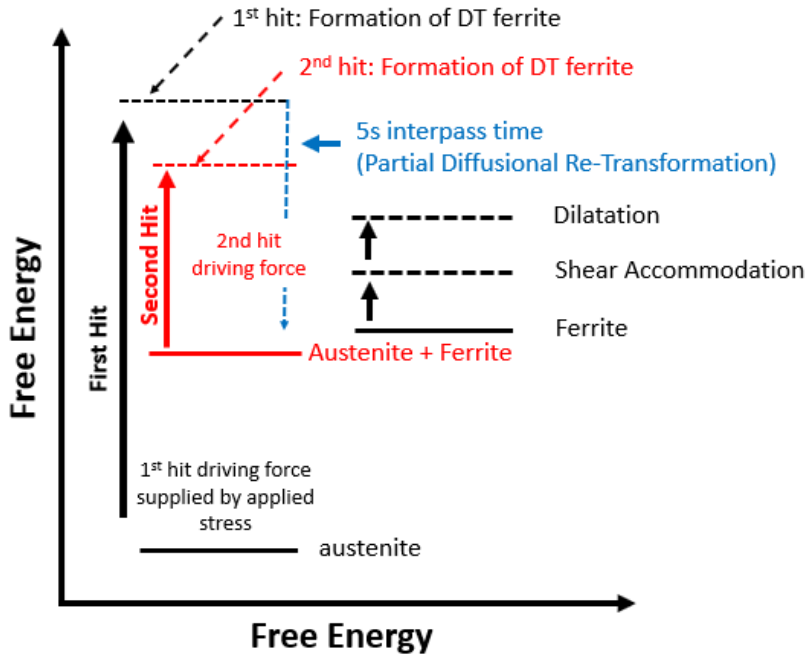

Figure 7: Schematic diagram of transformation mechanics during double hit hot deformation.

The present work focusses on the onset of the critical stress for the DT of austenite to ferrite during double hit deformation complemented with microstructural analysis to verify the observations. The following are conclusions from the present research.

1. The flow stress increases with the decrease in the temperature and increase in the strain rate for both temperatures and strain rates.
2. The critical stress associated with the onset of DT during the first deformation is higher than the critical stresses measured during the second hit deformation.
3. The critical stress increases with temperature and strain rates for both first and double hit deformations.

The authors acknowledge with gratitude funding received from the Natural Sciences and Engineering Research Council of Canada (NSERC), New Brunswick Innovation Foundation (NBIF) and Harrison McCain Foundation.

Authors have no conflict of interest relevant to this article

References:

1. Ghosh, C., C. Aranas Jr, and J.J. Jonas, *Dynamic transformation of deformed austenite at temperatures above the Ae3.* Progress in Materials Science, 2016. **82**: p. 151-233.
2. Yada, H., C.-M. Li, and H. Yamagata, *Dynamic γ→α Transformation during Hot Deformation in Iron–Nickel–Carbon Alloys.* ISIJ International, 2000. **40**(2): p. 200-206.
3. Yada, H., Y. Matsumura, and K. Nakajima, *Ferritic steel having ultra-fine grains and a method for producing the same*. 1984, Google Patents.
4. Basabe, V.V., J.J. Jonas, and C. Ghosh, *Formation of Strain-induced Ferrite in Low Carbon Steels at Temperatures Above the Ae₃.* ISIJ International, 2013. **53**(12): p. 2233-2241.
5. Essadiqi, E. and J.J. Jonas, *Effect of deformation on the austenite-to-ferrite transformation in a plain carbon and two microalloyed steels.* Metallurgical Transactions A, 1988. **19**(3): p. 417-426.
6. Ghosh, C., et al., *Dynamic Transformation Behavior of a Deformed High Carbon Steel at Temperatures Above the Ae₃.* ISIJ International, 2013. **53**(5): p. 900-908.
7. Chadha, K., et al., *Influence of strain rate on dynamic transformation of austenite in an as-cast medium-carbon low-alloy steel.* Materialia, 2018. **1**: p. 155-167.
8. Chadha, K., et al., *On the Role of Chromium in Dynamic Transformation of Austenite.* Metals and Materials International, 2019. **25**(3): p. 559-569.
9. Jonas, J.J., et al., *The Critical Strain for Dynamic Transformation in Hot Deformed Austenite.* ISIJ International, 2013. **53**(1): p. 145-151.
10. Ghosh, C., V.V. Basabe, and J.J. Jonas, *Determination of the Critical Strains for the Initiation of Dynamic Transformation and Dynamic Recrystallization in Four Steels of Increasing Carbon Contents.* steel research international, 2013. **84**(5): p. 490-494.
11. Poliak, E.I. and J.J. Jonas, *Initiation of dynamic recrystallization in constant strain rate hot deformation.* ISIJ International, 2003. **43**(5): p. 684-691.
12. Poliak, E.I. and J.J. Jonas, *A one-parameter approach to determining the critical conditions for the initiation of dynamic recrystallization.* Acta Materialia, 1996. **44**(1): p. 127-136.
13. Bale, C.W., et al. *Recent Developments in Factsage Thermochemical Software and Databases*. 2016. Cham: Springer International Publishing.
14. Aranas Jr, C., et al., *Flow Softening-based Formation of Widmanstätten Ferrite in a 0.06%C Steel Deformed Above the Ae₃.* ISIJ International, 2015. **55**(1): p. 300-307.
15. Poliak, E.I. and J.J. Jonas, *Critical strain for dynamic recrystallization in variable strain rate hot deformation.* ISIJ International, 2003. **43**(5): p. 692-700.

16. Grewal, R., et al., *Formation of Widmanstätten ferrite at very high temperatures in the austenite phase field.* Acta Materialia, 2016. **109**: p. 23-31.
17. Park, N., et al., *Occurrence of dynamic ferrite transformation in low-carbon steel above Ae3.* Scripta Materialia, 2013. **68**(7): p. 538-541.
18. Reick, W., M. Pohl, and A.F. Padilha, *Recrystallization–Transformation Combined Reactions during Annealing of a Cold Rolled Ferritic–Austenitic Duplex Stainless Steel.* ISIJ International, 1998. **38**(6): p. 567-571.
19. Aranas Jr, C. and J.J. Jonas, *Effect of Mn and Si on the dynamic transformation of austenite above the Ae3 temperature.* Acta Materialia, 2015. **82**: p. 1-10.